High Temperature Compressive Strength and Creep Behavior of Si-Ti-C-O Fiber-Bonded Ceramics

M. C. Vera[1], J. Martínez-Fernandez[1], M. Singh[2], J. Ramírez-Rico[1*]

[1] Dpto. Física de la Materia Condensada. Instituto de Ciencia de Materiales de Sevilla (ICMS). Universidad de Sevilla. Consejo Superior de Investigaciones Científicas (CSIC). Avda. Reina Mercedes S/N, 41012 Sevilla, Spain

[2] Ohio Aerospace Institute, 22800 Cedar Point Road, Cleveland, OH 44142, USA

Abstract

Fiber bonded silicon carbide ceramic materials provide cost-advantage over traditional ceramic matrix composites and require fewer processing steps. Despite their interest in extreme environment thermostructural applications no data on long term mechanical reliability other than static fatigue is available for them. We studied the high temperature compressive strength and creep behavior of a fiber bonded SiC material obtained by hot-pressing of Si-Ti-C-O fibers. The deformation mechanism and onset of plasticity was evaluated and compared with other commercial SiC materials. Up to 1400 °C, plasticity is very limited and any macroscopic deformation proceeds by crack formation and damage propagation. A transient viscous creep stage is observed due to flow in the silica matrix and once steady state is established, a stress exponent $n \sim 4$ and an activation energy $Q \sim 700$ kJ mol^{-1} are found. These results are consistent with previous data on creep of polymer derived SiC fibers and polycrystals.

Keywords: silicon carbide; ceramic matrix composites; creep; high temperature

* Corresponding author – Email: jrr@us.es, Tel: +34 954 550 936

1 Introduction

Silicon–based ceramic materials are candidates for a number of applications in energy production, storage, conservation, and efficiency fields due to their good thermal stability and low density, as well as creep resistance. In particular silicon carbide-based materials, due to their high temperature capability, low thermal expansion coefficient, and good thermal conductivity, as well as good fracture toughness when designed into a Ceramic Matrix Composite (CMC), have been developed and used in various applications such as gas turbines [1, 2], thermal management [3], nuclear fusion [4-7], aerospace [8] and braking systems [9]. The development of new CMCs has greatly benefited from the introduction of novel ceramic fibers with enhanced properties. In the case of SiC/SiC CMCs, there is a wide range of near oxygen-free silicon carbide fibers are available [10] and a variety of composites are in production and industrial use.

Even though CMCs are very interesting materials with numerous property attributes, their use in non-critical applications is not widespread due to the high processing costs associated with them. Ceramic laminates and fibrous monoliths [11] represent a low cost alternative with many of the advantages of CMCs such as increased toughness [12, 13], thermal shock resistance [14], lower creep rates [15], good wear behavior [16] or in-plane fracture resistance [17]. Fiber bonded ceramics are obtained by hot-pressing of ceramic mats, resulting in materials that can be considered halfway between CMCs and fibrous monoliths [18-22]. A significant advantage of this approach is that their production requires fewer processing steps than CMCs and they can be shaped into complex forms by means of molds and spacers, significantly reducing manufacturing costs. The green fiber mates used for fiber bonded ceramics can also be utilized for additive manufacturing using laminated object manufacturing (LOM) technology.

Despite their interesting properties and commercial application potential, detailed studies on high temperature mechanical properties of these materials are still limited. Matsunaga *et al.* studied creep rupture at temperatures up to 1500 °C and bending stresses up to 225 MPa in Si-Ti-C-O fiber bonded ceramics [23], while Kajii *et al*. evaluated 3-point bending strength. In a previous paper, we evaluated thermal stability and its impact on room temperature strength in Si-Al-C-O based ceramics and found the material to be able to withstand up to 1500 °C without degradation [24]. Several studies exist regarding the joining and integration of these materials

to themselves, to other ceramics and to metals, mostly through the use of brazing alloys [23, 25-27].

In this paper, we study the compressive strength and creep in Si-Ti-C-O fiber bonded ceramics in air at temperatures ranging from 1200 °C to 1500 °C. These studies are critically needed in order to establish the stress and temperature range at which plastic deformation can be significant since these materials contain a secondary glassy phase.

2. Materials and Methods

2.1 Si-Ti-C-O fiber bonded ceramics

The Si-Ti-C-O fiber bonded materials studied here were supplied by UBE Industries (Yamaguchi, Japan) under the *Tyrannohex* commercial brand as ingots of different shapes. Details of its processing have been published elsewhere [23]. In brief, continuous yarns of Si-Ti-C-O fibers are obtained from a poly titanocarbosilane polymer precursor [28, 29] that is melt-spun at 270 °C and cured at 170 °C and later pyrolyzed in N_2 atmosphere at temperatures ranging from 800 to 1500 °C [22]. The resulting Si-Ti-C-O fibers are then oxidized in air at 1000-1100 °C for 20h to obtain a 200-300 nm thick thermally grown oxide layer that will yield the matrix in the final composite. Oxidized fibers are then woven in 8-HS configuration and the resulting cloths cut and stacked in a shaper for hot pressing at 1750 °C in Ar at a pressure of 40 – 70 MPa [18]. This temperature is chosen to obtain fully dense monoliths and to induce crystallization in the SiC fibers: experiments showed that at 1600 °C much thicker SiO_2 layers were required to obtain dense monoliths [22]. During hot-pressing a thin carbon layer appears at the interface between the SiC and the SiO_2 thermally grown oxide layer, which is attributed to an excess C in the fiber precursor that diffuses towards the outer surface of the fibers during sintering. The oxide layer also contains small amounts of TiO_2 due to the initial Ti content in the fibers that react with the free carbon to form TiC particles. The final, dense ceramic consists of pressed Si-Ti-C-O fibers surrounded by a mostly amorphous SiO_2 layer with TiC precipitates [18, 19].

2.2 Microstructure and X-ray Diffraction

SEM observations were carried out in a Jeol 6460LV scanning electron microscope equipped with an EDS detector, using samples prepared by conventional metallographic procedures. TEM observations were carried out in a FEI Thalos microscope operating at 200 keV using

samples prepared as lamellas in a Zeiss Auriga dual beam FIB/SEM. X-ray diffraction was performed in a Bruker D8 Advance A25 diffractometer in a Bragg-Brentano configuration using Cu radiation. All these observations were carried out at the CITIUS central research facilities of the University of Sevilla.

2.3 Mechanical Testing

Samples for compression tests were cut as parallelepipeds with nominal dimensions (2x2x3) mm^3, using a low speed diamond wafering blade. Due to the shape and dimensions of the monoliths studied in this work, the compressive load was applied parallel to the pressing direction used in the hot-pressing procedure, which coincided with the longest dimension in the samples. It has been shown [24] that compressive strength tested in this direction is one order of magnitude higher than when tested in a direction contained in the sheet plane, as also happens in other SiC/SiC composites [30].

Compressive strength was measured using an electromechanical Universal Testing Machine (EM1/50/FR Microtest, Madrid) with an attached furnace, using high purity Al_2O_3 compressive rods. Polycrystalline α-SiC pads (Hexoloy, Saint Gobain Ceramic Materials, Köln) were used between rods and the samples. Samples were first tested at 1 μm min^{-1} crosshead speed which, for the sample dimensions used in this work, corresponded to a nominal initial strain rate of $\dot{\epsilon} = 5.5 \cdot 10^{-6}$ s^{-1}. These experiments were performed at temperatures in the range 1200 – 1450 °C in air.

Creep experiments were performed on identical samples using a dead weight loading creep testing equipment (M/SCM-2-FP, Microtest, Madrid) with an attached furnace. As before, load was applied using Al_2O_3 rods and SiC pads. Temperatures in the range 1400 – 1500 ºC were studied at nominal loads of 150 – 230 MPa. As will be explained below, long transient creep regimes and non-steady-state deformation at some of the testing conditions precluded us from performing dynamical changes in loading to obtain instantaneous creep parameters. Instead, each sample was studied at a single stress and temperature until we either detected failure or determined that steady-state was reached.

3 Results and discussion

3.1 Microstructure

The microstructure of the as received Si-Ti-C-O ceramic is shown in Figure 1. Fibers have diameters in the 7 – 9 μm range and are arranged in two perpendicular directions. Fiber sections are typically circular since plastic deformation during pressing takes place mostly in the oxide matrix. An EDS mapping (lower panels) confirms that fibers contain mostly Si and C while the matrix or interphase contains Si and O. Pore volume is very low, as measured density using a He-pycnometer was $\rho_{pyc} = (2.338 \pm 0.005)$ g cm^3, resulting in 2.6 vol. % pore volume when compared with the density of the fibers, which is larger but in line with previous reports [18, 22].

Transmission electron microscopy observations (Figure 2) show the presence of a turbostratic carbon interlayer between fibers and matrix 20-40 nm thick as well as TiC precipitates. These are attributed to a carbon excess as well as the presence of Ti in the fiber precursor, respectively. SiC crystallite size is very small with individual grains well below 100 nm. X-ray diffraction (Figure 3) from sections perpendicular (in plane) and parallel (out of plane) to the pressing direction reveal that SiC is very fine-grained and of the β polytype. The diffuse scattering from the matrix confirms its amorphous nature, although a small cristobalite peak is present in both orientations. TiC peaks could not be observed due to their small amount as well as the overlap of the cubic TiC peaks with those from SiC. The main difference between diffraction patterns in the *in-plane* and *out-of-plane* orientations is due to texture and the amount of surface SiO_2 present in the diffracting volume, depending on the measurement direction. In the out-of-plane direction the x-rays probe planes that are parallel to the fiber mats which are stacked and pressed together to form the monoliths, whereas in the in-plane direction the x-rays probe sections perpendicular to those. The amount of SiO_2 in the diffracting volume is larger in the first case, and that explains the larger amorphous background.

3.2 Compressive Strength

Strength and creep measurements were performed on samples cut into parallelepipeds with their largest direction parallel to the hot pressing direction, as depicted in Figure 4. This direction was chosen because in previous studies in similar materials [24] it was shown that

strength in this direction was an order of magnitude higher than in the perpendicular direction due to shearing of the individual fiber planes, as happens in similar composite materials [30].

Figure 5 shows the maximum measured compressive stress at each test, as a function of temperature. Strengths are in the range 250 – 450 MPa and decrease with temperature up to approximately 1350 °C and increases at higher temperatures, which can be attributed to a crack healing and defect blunting effect typical of SiC materials [31] and produced by SiO_2 formation and/or flow. Figure 6 shows stress-strain curves in compression measured at different temperatures, showing a behavior typical of CMCs that fracture by damage accumulation [32]. In this case, due to the presence of the vitreous interlayer between the fibers, there is plasticity even at moderately high temperatures. Thus, failure occurs by damage accumulation and propagation due to the material's inability to accommodate deformation. This is different to brittle fracture where the defect size distribution dictates strength and thus a large number of samples need to be tested. The shape of the stress-strain curves, which slope and curve downwards smoothly before failure rather than doing so abruptly corroborates this hypothesis, as does the fact that standard deviations for strength are low at all temperatures

Figure 7 shows images of the lateral faces of the samples after testing: while at 1200 °C cracks seem to propagate as they would do in a monolith, at 1250 °C open cracks tend to be perpendicular to the fibers instead of propagating in-between them to them. This could be due to the fact that SiO_2 is flowing and sealing the crack path, and this effect should be more pronounced in the case of cracks along planes parallel to the fibers, where the amount of SiO_2 the crack encounters should be higher.

One purpose of these compression tests was to establish a range in which plasticity and especially steady state creep could occur. A prerequisite is that damage accumulation in the range of studied temperatures and loads is negligible. In Figure 6, plastic effects are evident at temperatures 1400°C and higher, however the absence of damage mechanisms is not clear only from analyzing the stress-strain curves. For that reason, one test performed at 1450 °C was stopped right after the maximum stress was reached and the sample was unloaded and cooled down with a small contacting load to maintain its integrity. This sample is shown in Figure 8. As can be seen in panel A, some barreling of the sample has occurred due to friction at the surfaces contacting with the loading pads, while in B, C some small cracks are visible. For this

reason, we chose to perform our creep tests at temperatures 1400 °C and higher, using loads between 1/3 and 2/3 of the maximum compressive strength.

3.3 Creep Experiments

Figure 9 shows $\log \dot{\varepsilon} - \varepsilon$ creep curves for tests at different loads and temperatures. For samples crept at 1400 °C we were not able to reach the steady state before failure at 250 MPa, but instead a minimum in creep rate was reached after which deformation accelerated until failure in a process that is typically associated with damage propagation in the material. Also at 1400 °C we were not able to measure steady state creep at 150 MPa and 200 MPa because the creep rates fell below our testing apparatus sensitivity.

Creep deformation in Si-Ti-C-O fiber bonded ceramics probably proceeds first by viscous flow of the SiO_2 phase that resides in the fibers' interstices. Figure 10 shows an enrichment in O_2 at the outer surface of a crept sample that can be either due to SiC oxidation or to SiO_2 flow out of the sample. During creep at 1400 °C at least 20% deformation is required to reach steady state. Martinez-Fernandez *et al.* studied the creep behavior of several SiC/Si composites and found that plastic deformation starts in the Si phase and that grain boundary sliding in the SiC grains is required to accommodate this deformation [33]. Since below approximately 1500 °C the SiC diffusion coefficient is very low, there is not a significant deformation of the SiC grains themselves and the lack of accommodation mechanism results in a decreasing creep rate with increasing deformation out of the steady-state. This mechanism can also be responsible for transient creep in Si-Ti-C-O fiber bonded ceramics, although involving creep by viscous flow in the SiO_2 phase, a deformation mechanism which is typical of ceramics with a glassy interphase at the grain boundary [34]. Once the glassy phase is pushed out and the fibers contact each other, a steady state will be reached in which deformation proceeds by deformation inside the fibers themselves.

Ishikawa [10] compared the tensile creep resistance of Si-Al-C-O fibers with other fibers such as Hi-Nicalon-S or Sylramic, all of them highly crystalline and near-stoichiometric. Creep rates for individual fibers at 1400 °C are shown in Figure 11 along with our results for Si-Ti-C-O at different temperatures and applied loads. All the fibers included in the graph show a high creep resistance, with Hi-Nicalon showing lower creep rates than Sylramic and Tyranno-SA, attributed to the lower amount of residual oxygen in the Hi-Nicalon fiber, while the elements incorporated in Sylramic and Tyranno fibers as sintering aids also enhance diffusion at the grain boundaries thus increasing creep rate for a given load. Measured creep rates for Si-Ti-C-O

fiber bonded ceramics are close to Sylramic and Tyranno-SA rates, which is reasonable since the Tyranno-Lox fibers that compose the fiber bonded ceramic contain residual carbon and O_2 at the SiC grain boundaries inside the fibers. A phenomenological creep exponent of $n \sim 4$ was measured for the individual fibers, which is consistent with our results, although no deformation mechanism is proposed in previous works.

Steady state creep rates vs. reciprocal temperature are depicted in Figure 12 alongside values collected from the literature for large grained monolithic SiC materials. Compressive creep experiments carried out on α-SiC by Lane *et al.* [35] resulted in a creep exponent $n \sim 1.5$ which is compatible with a grain boundary sliding deformation mechanism. They observed a change in activation energy at ca. 1600 °C which was attributed to a change in the accommodation mechanism, from grain boundary diffusion alongside dislocations to bulk diffusion with enhanced dislocation activity. Creep resistance for Reaction Bonded Silicon Carbide (RBSC) materials is lower in all cases when tested in tension [36]. Our results for Si-Ti-C-O exhibit activation energies comparable to that of α-SiC at the high-temperature range, suggesting that creep may be controlled by bulk diffusion as well. Given the grain size in Si-Ti-C-O, it is not surprising that bulk diffusion can be relevant at much lower temperatures.

4 Conclusions

Si-Ti-C-O ceramics are interesting candidates for several high temperature applications due to their good combination of toughness, strength and near net shape processing. We have shown that they are also highly creep resistant, exhibiting strain rates in the range of $10^{-5} - 10^{-7}$ s^{-1} at temperatures of 1400-1500 °C, even though they exhibit long transient creep due to the presence of SiO_2 at the interface between the fibers. The large difference with respect to bulk SiC ceramics can be attributed to the much smaller grain size, which is of the order of 20-50 nm in these materials.

Acknowledgements

Part of this research was funded by the Spanish MINECO under grants MAT2013-41233-R and MAT2016-76526-R. Electron microscopy measurements were performed at the CITIUS central services of the University of Seville. Carmen Vera gratefully acknowledges support of the FPU program of the Spanish Ministerio de Educación, Cultura y Deporte.

References

[1] P. Baldus, M. Jansen, D. Sporn, Ceramic fibers for matrix composites in high-temperature engine applications, Science 285(5428) (1999) 699-703.
[2] A. Evans, Ceramics and Ceramic Composites as High-Temperature Structural Materials: Challenges and Opportunities [and Discussion], Philosophical Transactions of the Royal Society of London A: Mathematical, Physical and Engineering Sciences 351(1697) (1995) 511-527.
[3] D.B. Marshall, B.N. Cox, Integral textile ceramic structures, Annu. Rev. Mater. Res. 38 (2008) 425-443.
[4] M. Kotani, A. Kohyama, Y. Katoh, Development of SiC/SiC composites by PIP in combination with RS, Journal of nuclear materials 289(1) (2001) 37-41.
[5] Y. Hirohata, T. Jinushi, Y. Yamauchi, M. Hashiba, T. Hino, Y. Katoh, A. Kohyama, Gas permeability of SiC/SiC composites as fusion reactor material, Fusion engineering and design 61 (2002) 699-704.
[6] M. Ferraris, M. Salvo, V. Casalegno, S. Han, Y. Katoh, H. Jung, T. Hinoki, A. Kohyama, Joining of SiC-based materials for nuclear energy applications, Journal of Nuclear Materials 417(1) (2011) 379-382.
[7] R. Naslain, Design, preparation and properties of non-oxide CMCs for application in engines and nuclear reactors: an overview, Composites Science and Technology 64(2) (2004) 155-170.
[8] W. Krenkel, F. Berndt, C/C–SiC composites for space applications and advanced friction systems, Materials Science and Engineering: A 412(1) (2005) 177-181.
[9] W. Krenkel, B. Heidenreich, R. Renz, C/C-SiC Composites for Advanced Friction Systems, Advanced Engineering Materials 4(7) (2002) 427-436.
[10] T. Ishikawa, Advances in inorganic fibers, Adv Polym Sci, Springer2005, pp. 109-144.
[11] W. Clegg, K. Kendall, N.M. Alford, T. Button, J. Birchall, A simple way to make tough ceramics, Nature 347(6292) (1990) 455-457.
[12] P. Calvert, J. Cesarano, H. Chandra, H. Denham, S. Kasichainula, R. Vaidyanathan, Toughness in synthetic and biological multilayered systems, Philosophical Transactions of the Royal Society of London A: Mathematical, Physical and Engineering Sciences 360(1791) (2002) 199-209.
[13] H.M. Chan, Layered ceramics: processing and mechanical behavior, Annual review of materials science 27(1) (1997) 249-282.

[14] Y.-H. Koh, H.-W. Kim, H.-E. Kim, J.W. Halloran, Thermal shock resistance of fibrous monolithic Si 3 N 4/BN ceramics, J Eur Ceram Soc 24(8) (2004) 2339-2347.
[15] A.R. de Arellano-López, S. López-Pombero, A. Domínguez-Rodríguez, J.L. Routbort, D. Singh, K.C. Goretta, Plastic deformation of silicon nitride/boron nitride fibrous monoliths, J Eur Ceram Soc 21(2) (2001) 245-250.
[16] K. Goretta, D. Singh, T. Cruse, A. Erdemir, J. Routbort, F. Gutierrez-Mora, A. de Arellano-Lopez, T. Orlova, B. Smirnov, Si 3 N 4/BN fibrous monoliths: Mechanical properties and tribological responses, Materials Science and Engineering: A 412(1) (2005) 146-152.
[17] J.C. McNulty, M.R. Begley, F.W. Zok, In-Plane Fracture Resistance of a Crossply Fibrous Monolith, Journal of the American Ceramic Society 84(2) (2001) 367-75.
[18] T. Ishikawa, S. Kajii, K. Matsunaga, T. Hogami, Y. Kohtoku, Structure and properties of Si-Ti-C-O fibre-bonded ceramic material, Journal of Materials Science 30(24) (1995) 6218-6222.
[19] T. Ishikawa, S. Kajii, K. Matsunaga, T. Hogami, Y. Kohtoku, Microstructure and properties of Si-Ti-C-O fiber-bonded ceramics, Japan Society of Materials Science, Journal 45(6) (1996) 593-598.
[20] T. Ishikawa, S. Kajii, K. Matsunaga, T. Hogami, Y. Kohtoku, T. Nagasawa, A tough, thermally conductive silicon carbide composite with high strength up to 1600 degrees C in air, Science 282(5392) (1998) 1295-1297.
[21] T. Ishikawa, Crack-resistant Fiber-bonded Ceramic, Advanced Engineering Materials 1(1) (1999) 59-61.
[22] S. Kajii, T. Ishikawa, K. Matsunaga, Y. Kohtoku, A new type of fiber-bonded-ceramic material synthesized from pre-oxidized Si-Ti-C-O fiber, Adv Perform Mater 1(2) (1994) 145-155.
[23] T. Matsunaga, S. Kajii, K. Matsunaga, T. Ishikawa, H.T. Lin, M. Singh, Thermomechanical Performance of Si-Ti-C-O and Sintered SiC Fiber-Bonded Ceramics at High Temperatures, Int J Appl Ceram Tec 8(2) (2011) 273-281.
[24] J. Ramírez-Rico, J. Martínez-Fernández, M. Singh, Effect of oxidation on the compressive strength of sintered SiC-fiber bonded ceramics, Materials Science and Engineering: A 534 (2012) 394-399.
[25] T. Matsunaga, M. Singh, R. Asthana, H.T. Lin, S. Kajii, T. Ishikawa, Microstructure and mechanical properties of joints in sintered SiC fiber-bonded ceramics, Key Engineering Materials, Trans Tech Publ, 2011, pp. 9-14.

[26] M. Singh, T. Matsunaga, H.-T. Lin, R. Asthana, T. Ishikawa, Microstructure and mechanical properties of joints in sintered SiC fiber-bonded ceramics brazed with Ag–Cu–Ti alloy, Materials Science and Engineering: A 557 (2012) 69-76.
[27] R. Asthana, M. Singh, H.T. Lin, T. Matsunaga, T. Ishikawa, Joining of SiC Fiber-Bonded Ceramics using Silver, Copper, Nickel, Palladium, and Silicon-Based Alloy Interlayers, Int J Appl Ceram Tec 10(5) (2013) 801-813.
[28] T. Yamamura, T. Ishikawa, M. Shibuya, T. Hisayuki, K. Okamura, Development of a new continuous Si-Ti-C-O fibre using an organometallic polymer precursor, Journal of Materials Science 23(7) (1988) 2589-2594.
[29] T. Ishikawa, T. Yamamura, K. Okamura, Production mechanism of polytitanocarbosilane and its conversion of the polymer into inorganic materials, Journal of Materials Science 27(24) (1992) 6627-6634.
[30] K.K. Chawla, Ceramic Matrix Composites, Springer, New York, 2003.
[31] R.G. Munro, Material properties of a sintered α-SiC, Journal of Physical and Chemical Reference Data 26(5) (1997) 1195-1203.
[32] K.K. Chawla, Composite Materials. Science and Engineering, Springer-Verlag New York, New York, 1998.
[33] J.M. Fernández, A. Munoz, A. de Arellano López, F.V. Feria, A. Dominguez-Rodriguez, M. Singh, Microstructure–mechanical properties correlation in siliconized silicon carbide ceramics, Acta Materialia 51(11) (2003) 3259-3275.
[34] J. Ramírez-Rico, Martínez-Fernández, M., High-Temperature Mechanical Behaviour of Hard Ceramics, Comprehensive Hard Materials, Elsevier Ltd.2014, pp. 321-324.
[35] J.E. Lane, C.H. Carter, R. Davis, Kinetics and Mechanisms of High-Temperature Creep in Silicon Carbide: III, Sintered α-Silicon Carbide, Journal of the American Ceramic Society 71(4) (1988) 281-295.
[36] R.E. Tressler, McNallan, M, Performance verification of new, low cost ceramics., J. R. Hellmann & B. K. Kennedy. Proyects within the center for advanced materials (1989).

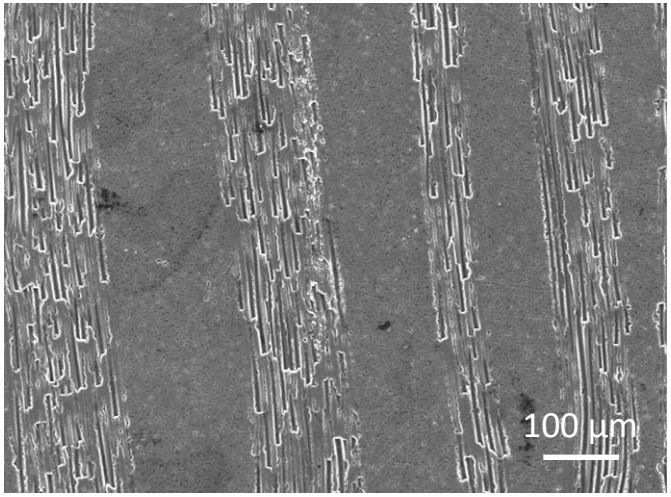

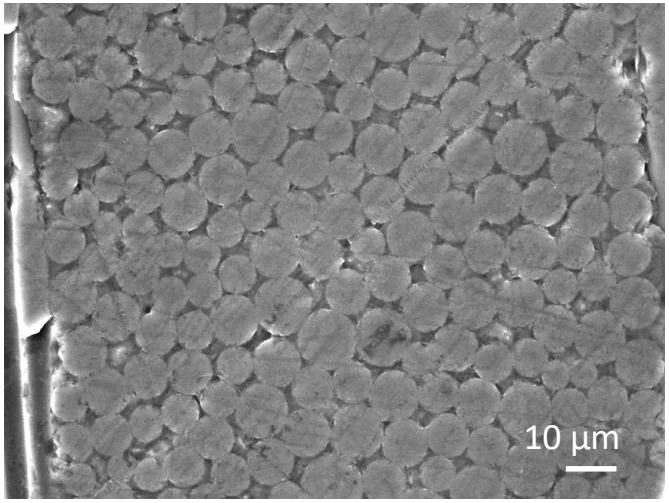

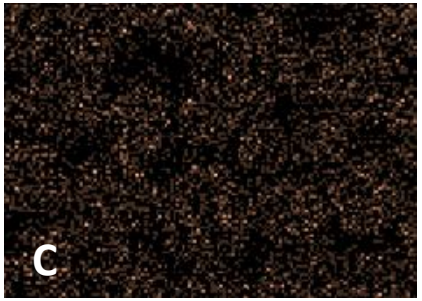

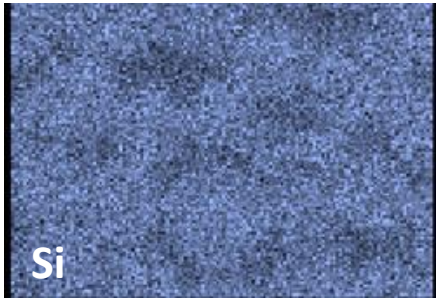

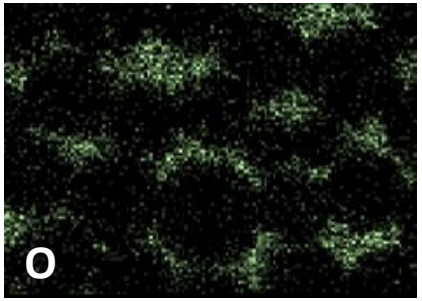

Figure

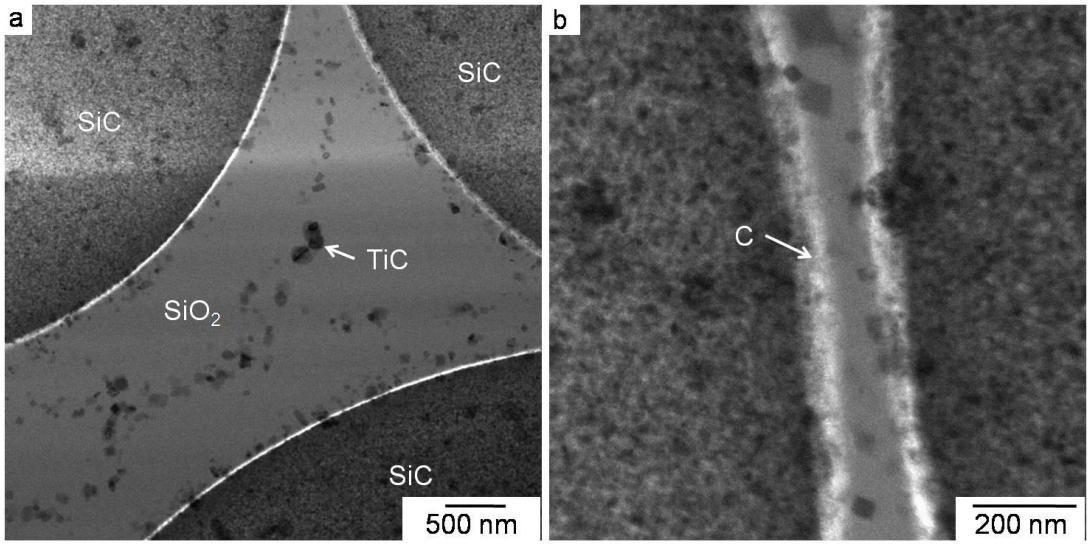

Figure

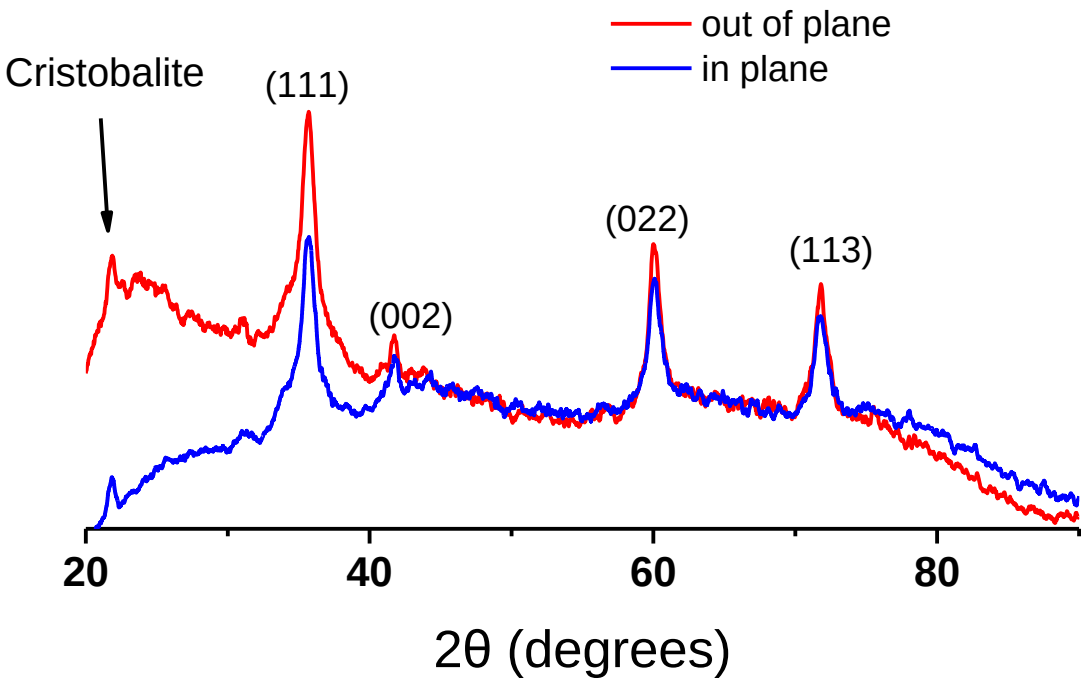
out of plane
in plane
Cristobalite
(111)
(002)
(022)
(113)
20
40
60
80
2θ (degrees)

Figure

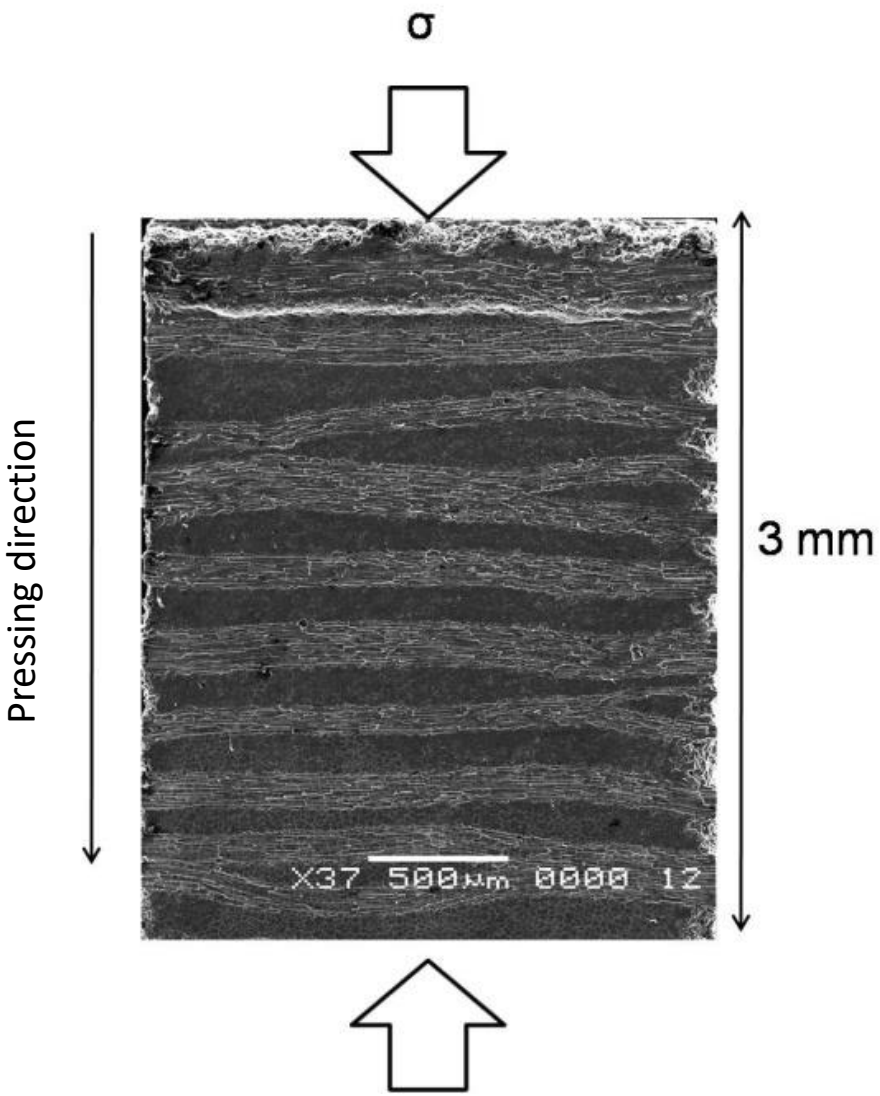

Figure

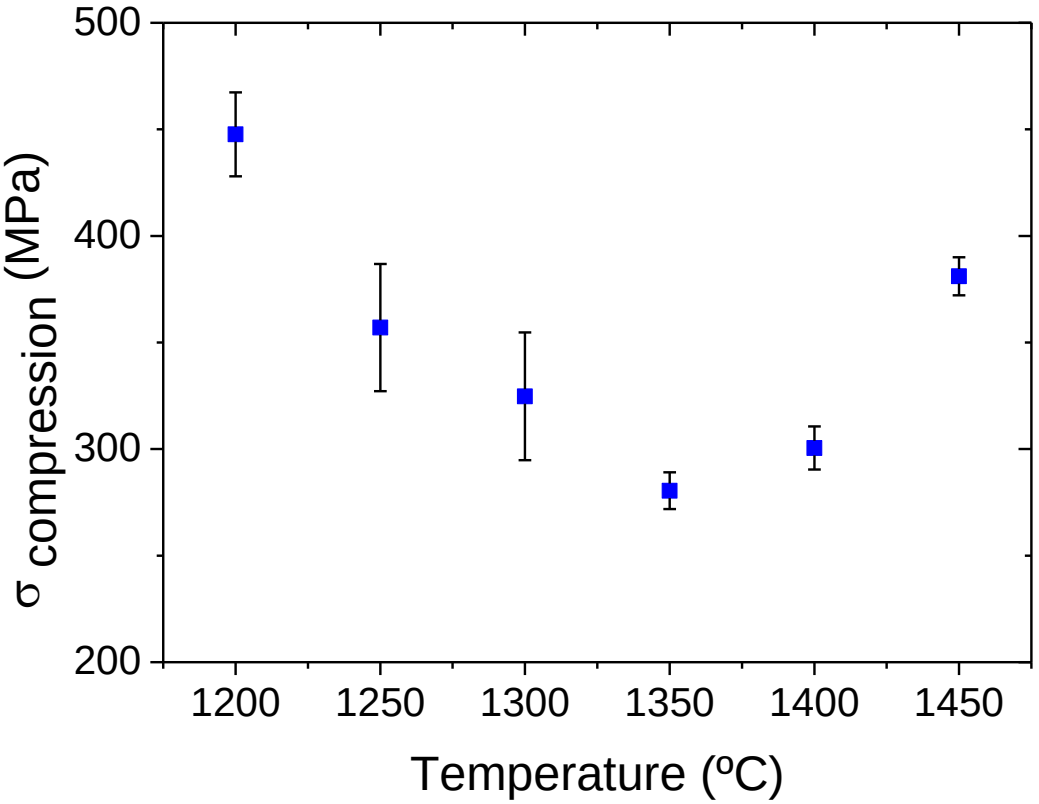
500
400
300
200
σ compression (MPa)
1200
1250
1300
1350
1400
1450
Temperature (ºC)

Figure

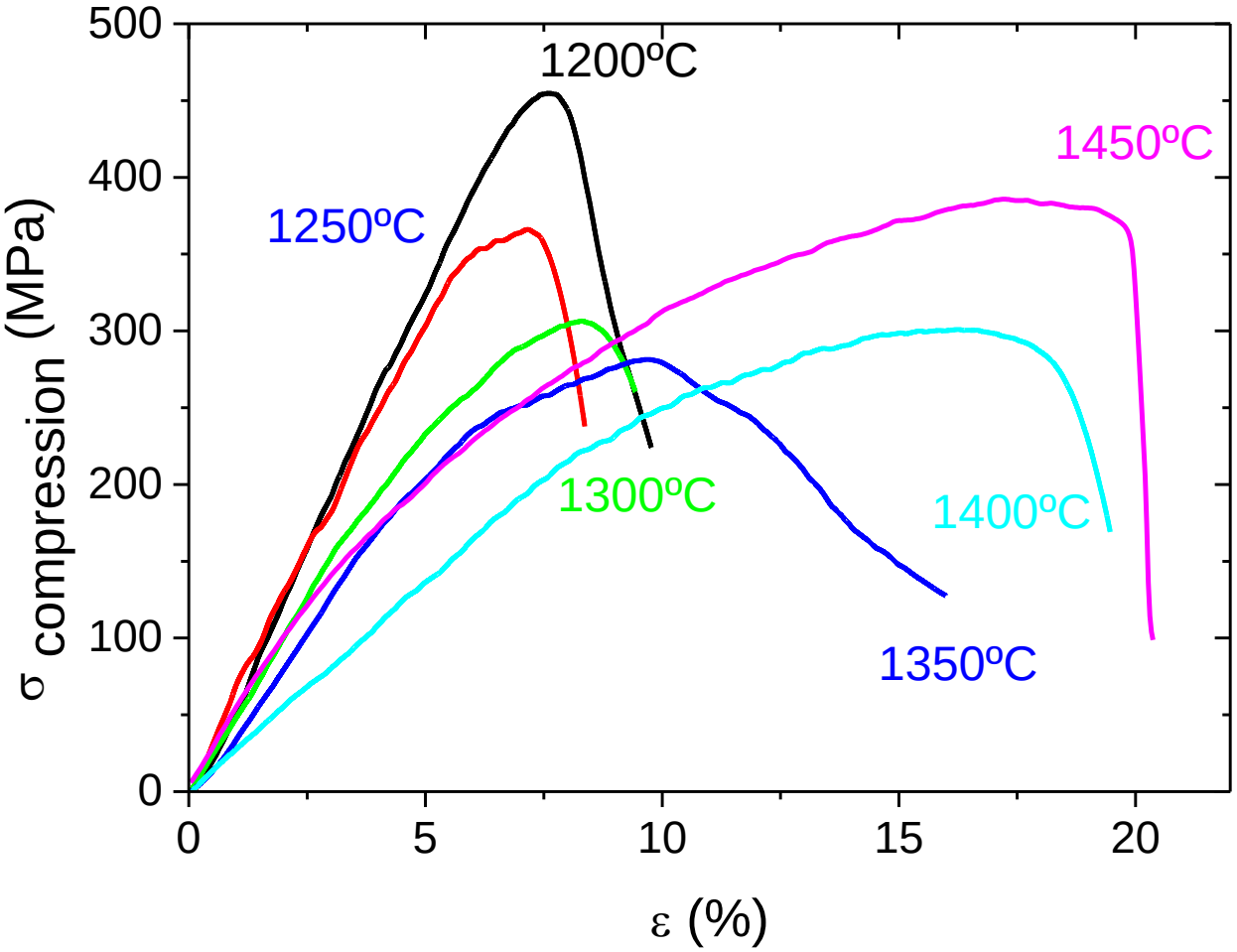
500
400
300
200
100
0
σ compression (MPa)
0
5
10
15
20
ε (%)
1200ºC
1450ºC
1250ºC
1300ºC
1400ºC
1350ºC

Figure

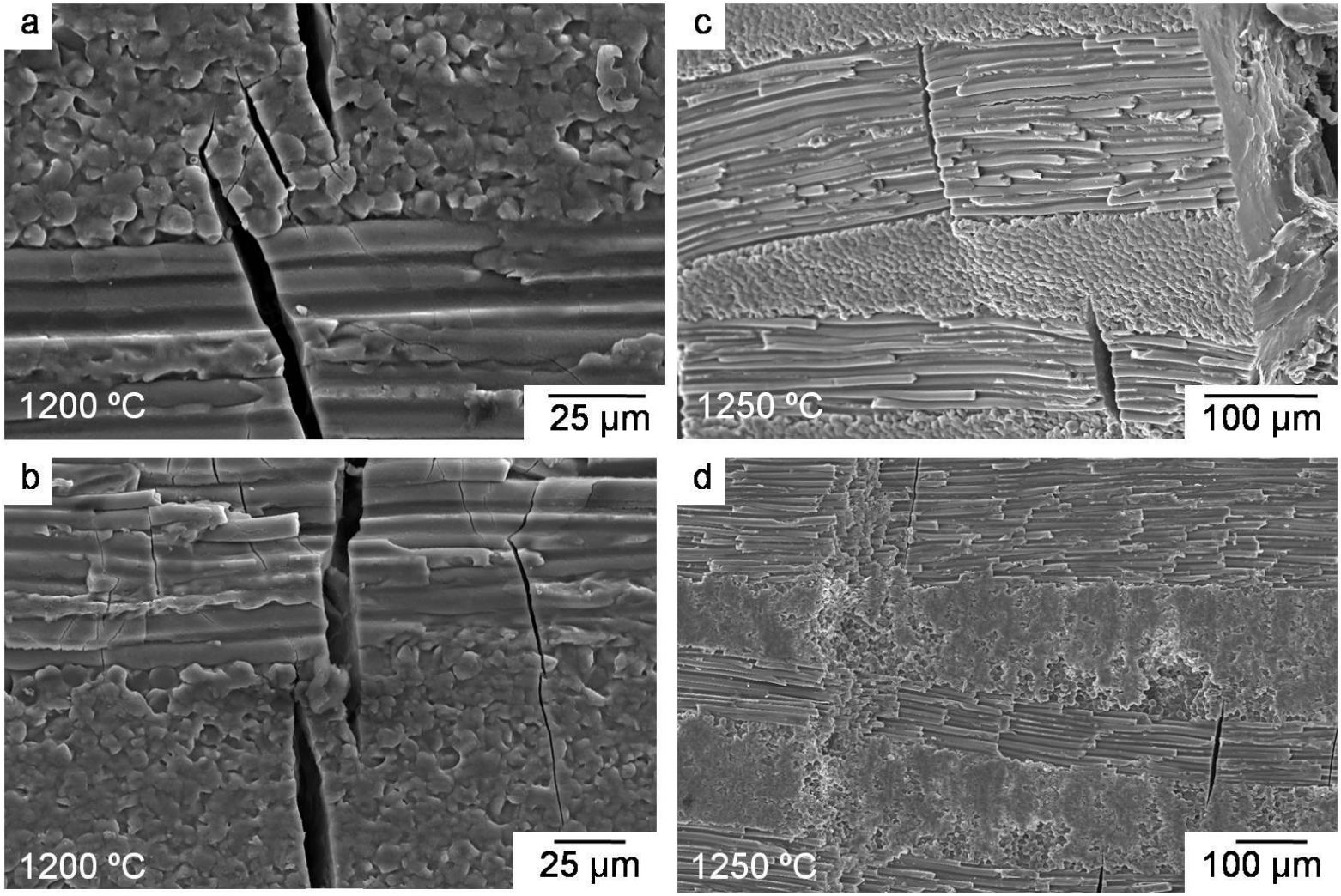

Figure

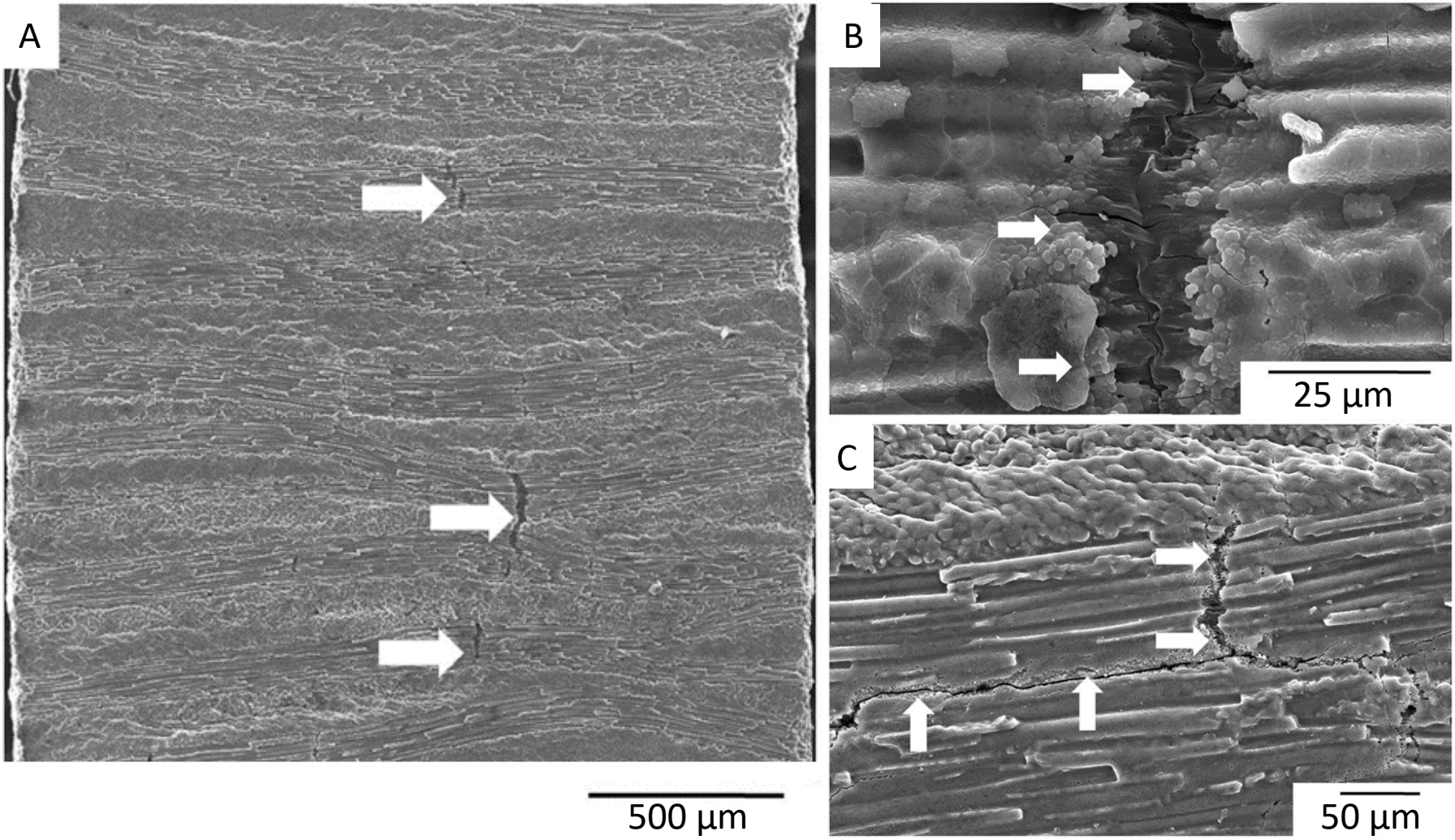

Figure

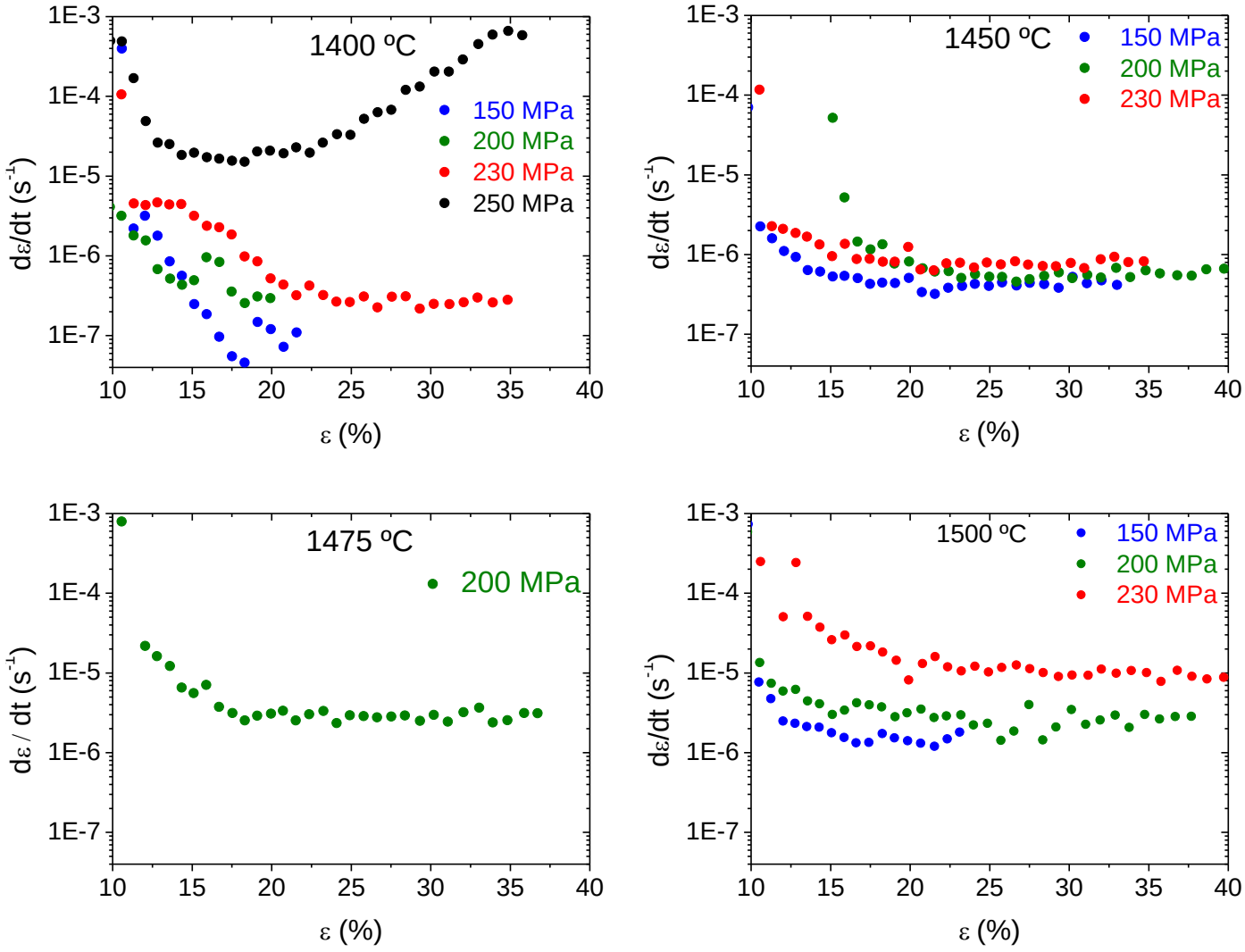
1400 ºC
150 MPa
200 MPa
230 MPa
250 MPa
1450 ºC
150 MPa
200 MPa
230 MPa
1475 ºC
200 MPa
1500 ºC
150 MPa
200 MPa
230 MPa
dε/dt (s⁻¹)
dε / dt (s⁻¹)
ε (%)
1E-3
1E-4
1E-5
1E-6
1E-7
10
15
20
25
30
35
40

Figure

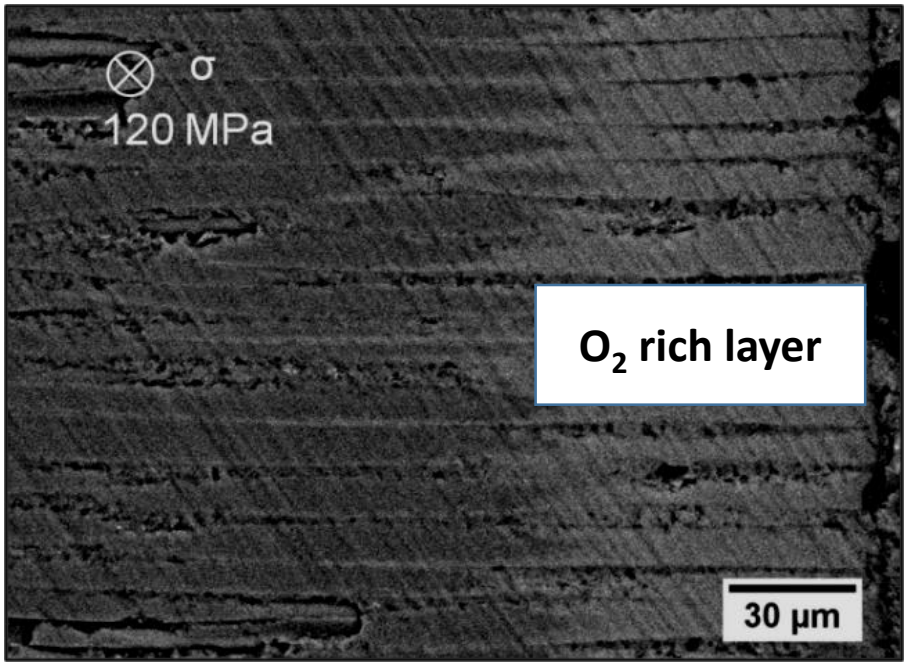

Figure

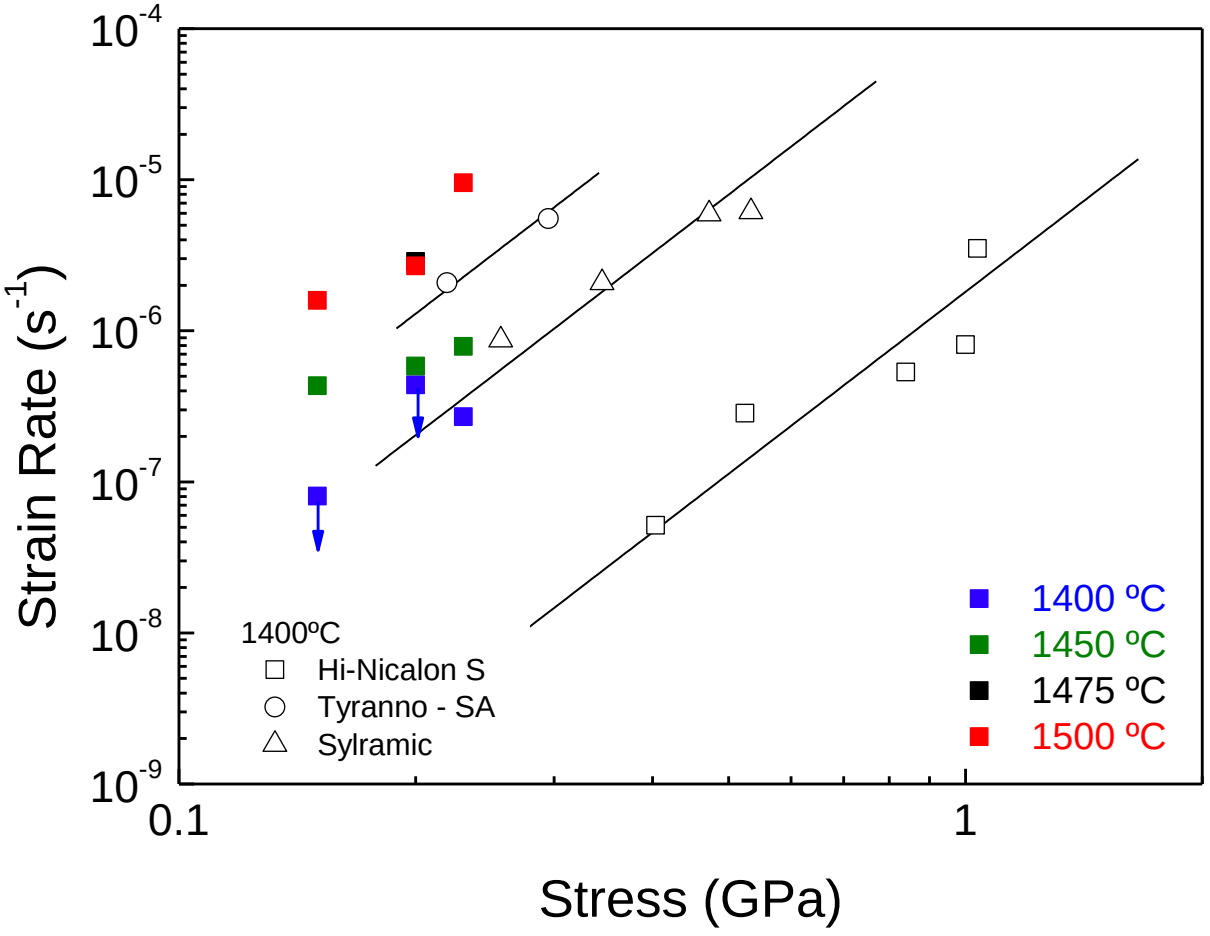
Strain Rate (s-1)
10-4
10-5
10-6
10-7
10-8
10-9
0.1
1
Stress (GPa)
1400ºC
Hi-Nicalon S
Tyranno - SA
Sylramic
1400 ºC
1450 ºC
1475 ºC
1500 ºC

Figure

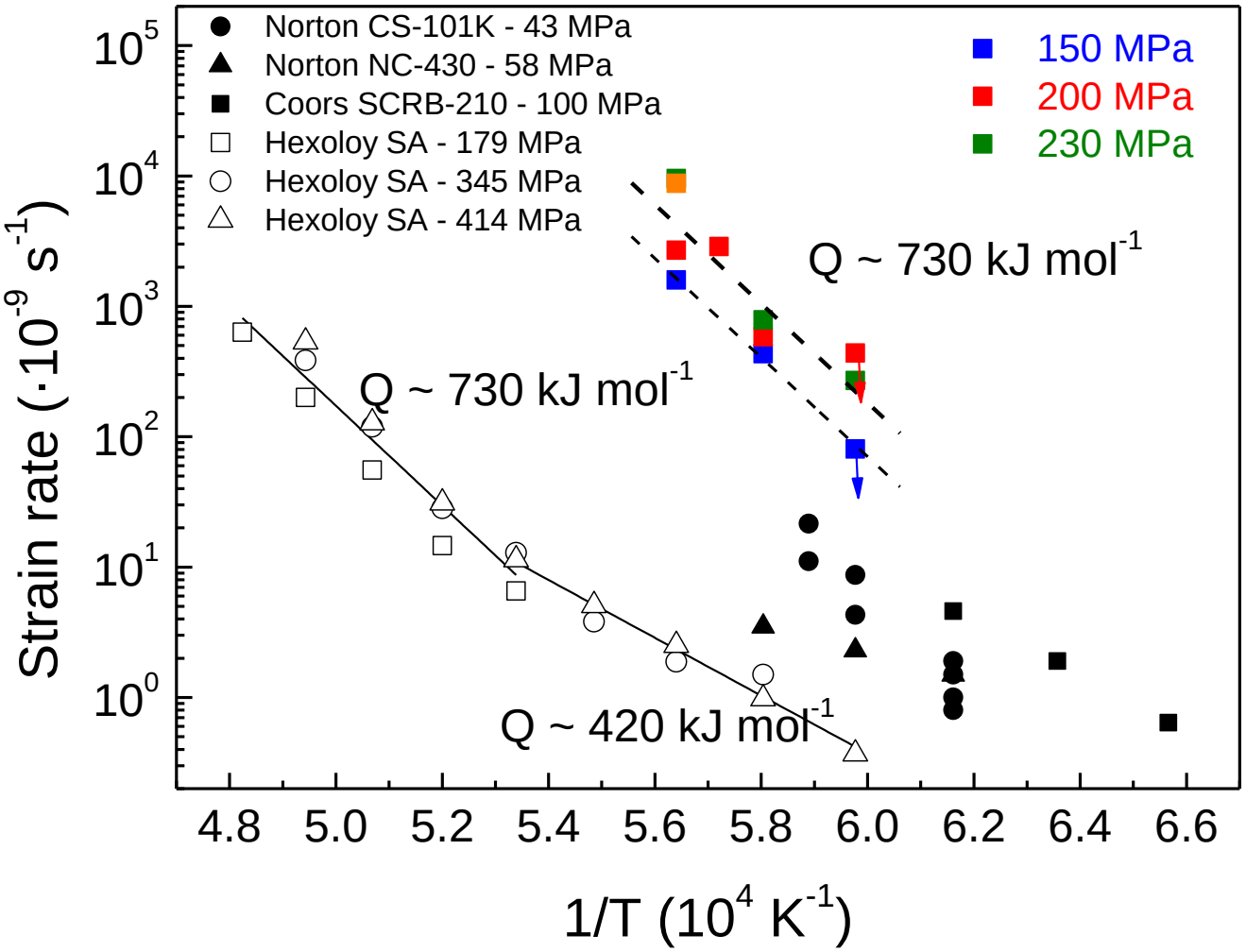
Norton CS-101K - 43 MPa
Norton NC-430 - 58 MPa
Coors SCRB-210 - 100 MPa
Hexoloy SA - 179 MPa
Hexoloy SA - 345 MPa
Hexoloy SA - 414 MPa
150 MPa
200 MPa
230 MPa
Q ~ 730 kJ mol-1
Q ~ 730 kJ mol-1
Q ~ 420 kJ mol-1
Strain rate (·10-9 s-1)
1/T (10^4 K-1)
10^5
10^4
10^3
10^2
10^1
10^0
4.8
5.0
5.2
5.4
5.6
5.8
6.0
6.2
6.4
6.6

Figure